A transcriptome-wide meta-analysis reveals lack of cancer-cell intrinsic determinants of response to immune checkpoint blockade

Yu Amanda Guo[1], Tanmay Kulshrestha[1], Mei Mei Chang[1], Irfahan Kassam[1], Egor Revkov[1,2], Simone Rizzetto[1], Aaron C. Tan[3], Daniel S.W. Tan[1,3], Iain Beehuat Tan[1,3] & Anders Jacobsen Skanderup[1,2,3]

[1]Genome Institute of Singapore (GIS), Agency for Science, Technology and Research (A*STAR), 60 Biopolis Street, Genome, Singapore 138672, Republic of Singapore

[2]School of Computing, National University of Singapore, Computing 1, 13 Computing Drive, Singapore 117417, Republic of Singapore

[3]National Cancer Centre Singapore, Singapore 168583, Republic of Singapore.

Correspondence should be addressed to A.J.S. (skanderupamj@gis.a-star.edu.sg)

Declaration of interests

The authors declare no competing interests.

Abstract

Immune-checkpoint therapy (ICB) has conferred significant and durable clinical benefit to some cancer patients. However, most patients do not respond to ICB, and reliable biomarkers of ICB response are needed to improve patient stratification. Here, we performed a transcriptome-wide meta-analysis across 1,486 tumors from ICB-treated patients and tumors with expected ICB outcomes based on microsatellite status. Using a robust transcriptome deconvolution approach, we inferred cancer and stroma-specific gene expression differences and identified cell-type specific features of ICB response across cancer types. Consistent with current knowledge, stromal expression of *CXCL9*, *CXCL13*, and *IFNG* were the top determinants of favorable ICB response. In addition, we identified a group of potential immune-suppressive genes, including *FCER1A*, associated with poor response to ICB. Strikingly, PD-L1 expression in stromal cells, but not cancer cells, is correlated with ICB response across cancer types. Furthermore, the unbiased transcriptome-wide analysis failed to identify cancer-cell intrinsic features of ICB response conserved across tumor types. Overall, our results challenge the prevailing dogma that cancer cells present tissue-agnostic molecular markers that modulate immune activity and ICB treatment response. These results have implications for the development of improved ICB treatments and diagnostics.

39 **Introduction**

40 Immune checkpoint blockade therapy (ICB) is an established class of immunotherapy that
41 induces significant tumor shrinkage and long-term disease control in many cancers.
42 However, only a subset of patients benefit from ICB, with response rates ranging from 0-3%
43 in pancreatic cancer[1] to about 40% in melanoma and microsatellite instable (MSI) tumors[2].
44 Presently, the Food and Drug Administration (FDA)-approved biomarkers for ICB are PD-L1
45 expression[3], microsatellite instability[4], and high tumor mutation burden (TMB)
46 of >10mutations/Mb[5]. While PD-L1 expression is an obvious biomarker for PD-1/PD-L1
47 blockade therapies, it is only weakly predictive of treatment response in many solid cancer
48 types[6]. TMB is a measure of tumor immunogenicity, where increased mutation load is
49 associated with higher neo-antigen burden and anti-tumoral immune responses. However,
50 the predictive power of TMB varies significantly by cancer type and it is difficult to define a
51 single TMB threshold across cancer types[7,8]. Likewise, MSI tumors are more immunogenic,
52 as defective mismatch repair results in large numbers of insertions and deletions in the
53 cancer genomes. In practice, MSI status has limited applications as a biomarker of ICB
54 response, since only a small subset of solid tumors are microsatellite instable[9,10].

55 Transcriptional signatures of tumor immune phenotypes have been proposed to
56 predict for ICB response[11-13]. However, analysis of large-scale ICB trial data found that
57 existing transcriptional signatures often have limited predictive accuracy in new patient
58 cohorts[6]. Two recent meta-analyses investigated the genomic and transcriptomic predictors
59 of ICB response[14,15]. Litchfield et al.[14] evaluated previously described biomarkers of ICB
60 response, and found TMB and *CXCL9* expression as the most consistent predictors of ICB
61 response. Bareche et al. performed a comparative analysis of existing gene signatures of ICB
62 response, and proposed a new predictive gene signature [15]. However, existing large-scale

63 studies have been restricted to bulk tumor transcriptomic data, providing limited insights
64 into the roles of cancer and stroma cells in the tumor microenvironment (TME) during ICB
65 therapy.

66 Activation of effector immune cells such as T-cells and natural killer (NK) cells are
67 dependent on a balance of co-stimulatory and co-inhibitory interactions between these
68 effector cells, antigen-presenting immune cells such as dendritic cells and macrophages, as
69 well as cancer cells in the TME. Dysregulation of these ligand-receptor interactions, or
70 immune checkpoints, leads to immunosuppression in the tumor. However, it is challenging
71 to tease apart these complex interactions between cancer and immune cells using bulk
72 tumor transcriptomics. For example, although inhibitory immune checkpoint ligand PD-L1 is
73 a known biomarker of ICB response, it is unclear if cancer cells escape immune cell killing by
74 expressing PD-L1, or recruiting PD-L1^{+} immune cells, with studies supporting both
75 scenarios[16]. Therefore, learning the cell type specificities of ICB biomarkers can provide
76 insights on the underlying mechanisms of immune evasion and ICB resistance. While single-
77 cell transcriptomics has been applied to explore immune cell types and molecular
78 mechanisms associated with ICB response, single cell transcriptomics studies are currently
79 limited to small patient cohorts[17,18]. The small sample size, coupled with high intra- and
80 inter- patient heterogeneity and intrinsic noise in single-cell data, limits the power of single-
81 cell transcriptomics for systematic biomarker discovery.

82 To study features of ICB response in cancer cells as well as in their neighboring
83 stromal cells, we applied a transcriptome deconvolution technique to estimate stroma- and
84 cancer-cell-specific expression of individual genes from bulk tumor transcriptomes. We used
85 a robust and validated non-negative least squares approach[19], which have previously been
86 applied across 8,000 TCGA tumors from 20 solid cancer types to uncover ligand-receptor

87 crosstalk and metabolic states of cancer and stroma cells in the TME[20 21]. Here, we applied
88 this transcriptome deconvolution technique to study the differential expression signatures
89 of ICB responders and non-responders in cancer and stroma cells. Using a cohort of 1,486
90 tumors with clinically annotated ICB response and tumors with expected ICB outcomes
91 based on microsatellite status., our analysis revealed a lack of cancer-cell intrinsic gene
92 expression signatures associated with ICB response across tumor types. In contrast, in
93 stromal cells, we identified multiple immunomodulators and checkpoint genes recurrently
94 associated with ICB response across cohorts and tumor types. Many of these genes have
95 previously been linked with ICB response and we uncovered a subset of novel and
96 potentially immune-suppressive genes negatively correlated with response. Using these
97 conserved stromal-specific gene signatures, we developed a compact 3-feature predictive
98 model of ICB response that demonstrated improved accuracy over existing biomarkers in
99 unseen patient cohorts and tumor types.
100
101

102 **Results**

103 **Patient cohorts used for transcriptome-wide analysis of ICB response**

104 To systematically explore transcriptome-wide biomarkers of ICB response, we obtained
105 transcriptome data for 534 tumors, comprising 4 ICB-treated patient cohorts from 3 tumor
106 types (gastric cancer[22], urothelial cancer[23] and melanoma[24,25]; **Figure 1**, **Supplementary**
107 **Table 1,** and **Methods**). Since about half of MSI tumors are expected to respond to ICB, as
108 compared to <10% in microsatellite stable (MSS) tumors[2,26,27], we further supplemented
109 the discovery cohort using large cohorts of treatment-naïve MSI/MSS tumors. We obtained
110 the transcriptomic profiles of 952 tumors from 3 tumor types in TCGA with the highest
111 frequency of MSI tumors (colorectal cancer, gastric cancer and endometrial cancer, **Figure**
112 **1**). As Epstein–Barr virus (EBV)-positive gastric tumors are also enriched for ICB
113 responders[22,27], we grouped MSI and EBV tumors together as the responder-enriched group
114 for gastric cancer. In total, the discovery cohort comprised of 1,486 tumors from 5 cancer
115 types.

116

117 **Tumor transcriptome deconvolution to identify features of ICB response in cancer and**
118 **stromal cells**

119 We performed tumor transcriptome deconvolution to estimate the stromal- and cancer-cell
120 expression of each gene in tumors from responders (MSI) and non-responders (MSS) (**Figure**
121 **1**). Briefly, we first used a consensus-approach to infer tumor purities based on
122 transcriptomic and genomic data (where available, Methods). For each ICB response group,
123 we estimated gene expression levels in stromal and cancer cells using a non-negative least
124 squares regression approach[20,21]. Finally, we identified cancer/stromal-cell differentially

125 expressed genes (DEGs) between ICB responders and non-responders using a permutation-
126 based statistic (**Figure 1, Supplementary Figure 1**).
127
128 **Top stromal genes associated with ICB response are enriched in immune pathways**
129 From this unbiased transcriptome-wide analysis, we identified 59 genes with differential
130 expression in stromal cells across all cohorts and tumor types (**Figure 2A-B, Supplementary**
131 **Figure 2A and 2C, Methods**). Among these DEGs, 51 (86%) had immune-related functions as
132 defined by the Gene Ontology (GO; see Methods), significantly higher than random
133 expectation (p < 2.2e-16, Fisher's Exact test). Stromal DEGs include genes involved in:
134 immune checkpoint signaling (e.g. *CD274*, *LAG3*, *CTLA4*), interferon gamma signaling (e.g.
135 *IFNG*, *IRF1*, *STAT1*), T-cell effector function (e.g. *PRF1*, *GZMA*, GZMB), and NK-cell mediated
136 cytotoxicity (*KLRD1*, *KLRC2*). Next, we performed pathway analysis to quantify the
137 enrichment of specific biological functions among the stromal DEGs associated with ICB
138 response. We identified 31 enriched GO biological process terms, all of which were immune
139 related (**Figure 2C**). These 31 terms could be further grouped into 4 clusters based on
140 similarity (see Methods): T cell activation, chemokine signaling, interferon-gamma response,
141 and natural killer cell mediated cytotoxicity **(Figure 2D**).
142 The top-2 DEGs with the greatest overexpression in ICB responders were
143 chemokines *CXCL9* and *CXCL13*. *CXCL9* is responsible for T-cell trafficking through binding
144 the *CXCR3* receptor on T-cells and has been associated with increased T-cell infiltration in
145 tumors[28]. *CXCL13* is involved in both B-cell and T-cell migration via binding to the *CXCR5*
146 receptor. Production of *CXCL13* by T follicular helper cells (T_{FH}) is essential for tertiary
147 lymphoid structure formation at tumor sites as well as germinal center B cell activation[29],
148 which has been linked with anti-tumoral response to ICB[30]. Consistent with our meta-

149 analysis, recent studies have also proposed *CXCL9* and *CXCL13* as key predictors of improved
150 ICB response[31,32]. Remarkably, these two chemokines were also highlighted by a recent
151 meta-analysis that evaluated existing biomarkers of ICB response[14], suggesting that *CXCL9*
152 and *CXCL13* are indeed the strongest individual transcriptomic predictors of ICB response
153 independent of tumor type.
154
155 **Stromal genes negatively associated with ICB response**
156 Although high immune infiltration is generally associated with better ICB response[11,33,34],
157 our analysis uncovered a group of immune-related genes consistently associated with poor
158 ICB outcomes across tumor types. Among these genes, *FCER1A* showed the strongest and
159 most consistent overexpression in ICB non-responders. *FCER1A* encodes a subunit of the IgE
160 receptor. While *FCER1A* is an established marker of basophils, mast cells and dendritic cells,
161 it is also expressed on immunosuppressive M2 macrophages[35] and tumor associated
162 macrophages (TAMs)[36]. *CH25H*, a gene encoding enzyme cholesterol 25-hydroxylase that
163 catalyzes the formation of 25-hydroxycholesterol (25-HC), was also up-regulated in tumors
164 of ICB non-responders. Interestingly, 25-HC is produced by macrophages in response to
165 type-I interferon signalling and has numerous immunological effects including B-cell
166 chemotaxis, macrophage differentiation, and regulation of inflammatory response[37]. We
167 also observed two natriuretic peptides, NPR1 and NPR3, among genes up-regulated in ICB
168 non-responders. Although natriuretic peptides function primarily to regulate electrolytes,
169 they are expressed in immune cells and there is increasing evidence of their role in
170 inflammation and immunity[38].
171

172 **Immune cell subtype analysis identifies M1 macrophages as strong correlate of ICB**
173 **response**

174 To identify immune cell populations associated with ICB response, we estimated the
175 immune cell composition of each tumor using Cibersortx[39] and compared the abundance of
176 immune cell subsets between ICB responders and non-responders. M1 macrophages, T-
177 follicular helper (Tfh), and activated CD4 memory T-cells had higher abundance in ICB
178 responders as compared to non-responders (**Figure 3A, Supplementary Figure 3**). M1
179 macrophages are known to be pro-inflammatory and anti-tumoral[40]. A recent study found
180 M1 macrophage infiltration to be predictive to ICB response in urothelial cancer[41]. Our
181 results further demonstrate that M1 macrophage infiltration could be a general feature of
182 ICB response across multiple cancer types. Tfh cells are specialized CD4+ T cells that aid the
183 formation of germinal centers in tertiary lymphoid structures (TLS)[42], interacting with B-cells
184 to activate antibody responses[43] and enhancing CD8+ T-cell effector functions[44]. While the
185 presence of Tfh cells has been associated with favorable survival in multiple cancer
186 types[30,43-45], their putative role in ICB response has not been studied. Our analysis also
187 demonstrated that while resting CD4 memory T-cells were enriched in non-responders,
188 activated CD4 memory T-cells were enriched in ICB responders. This suggests that pre-
189 existing CD4+ T-cell immunity is important for effective anti-tumoral response upon ICB
190 treatment.

191 Next, we examined associations between the top DEGs and infiltration of specific
192 immune cell subsets. We found that the top gene expression markers of good ICB response
193 were generally associated with abundance of M1 macrophages, CD4+/CD8+ T-lymphocytes,
194 and activated NK cells (**Figure 3B, Supplementary Figure 4**). Using orthogonal expression
195 data of immune cells subtypes from flow cytometry and single-cell RNA-seq experiments,

196 we confirmed that *CXCL9* expression was strongly associated with M1 macrophage
197 infiltration, while *CXCL13* and *IFNG* expression were strongly associated with T-cell
198 infiltration (**Supplementary Figure 5**). Interestingly, the DEGs associated with poor ICB
199 response, including FCER1A, were correlated with resting state of mast cells, CD4+ memory
200 T cells, and dendritic cells, suggesting that these genes are likely markers of a quiescent or
201 immune-suppressive microenvironment (**Figure 3B, Supplementary Figure 4**).
202
203 **Cancer intrinsic features of ICB response tend to be tumor type specific**
204 Previous studies have proposed multiple mechanisms by which cancer cells may directly
205 suppress tumor immunity and impede ICB therapy[16,46]. Surprisingly, our meta-analysis
206 across tumor types revealed a paucity of DEGs associated with ICB response in cancer cells.
207 In cancer cells, we identified 9 genes differentially expressed between ICB responders and
208 ICB non-responders across tumor types (**Figure 4A, Supplementary Figure 2B & D**). In
209 addition, we observed that the differential expression signal for these 9 genes was mostly
210 driven by the MSI ICB-responder-enriched cohorts. As compared to stromal DEGs (**Figure**
211 **2A**), the signal for the cancer DEGs was less consistent across the distinct ICB cohorts (**Figure**
212 **4A**). Therefore, we hypothesize that the cancer DEGs identified by the meta-analysis are
213 likely related to biology of MSI tumors, rather than general mechanisms of ICB response. We
214 also confirmed that the paucity of cancer cell DEGs, as compared to stroma cell DEGs,
215 persisted regardless of the significance cutoff in our meta-analysis (**Figure 4B**), and we were
216 not able to identify functional enrichment or relationships among cancer DEGs.
217 Next, we conducted the same DEG analysis within individual tumor types to explore
218 the potential for tissue-dependent processes involved in ICB response. For melanoma, we
219 only identified 22 cancer DEGs shared between the 2 melanoma cohorts, and these genes

220 were not enriched in specific pathways. In gastric cancer, we identified 190 cancer ICB
221 response DEGs across the gastric ICB cohort and TCGA cohort. Interestingly, genes
222 associated with poor ICB response were enriched for angiogenesis-related functions (**Figure**
223 **4C**), with pro-angiogenic genes ENG, F2R and PDGFRB overexpressed in ICB non-responders
224 (MSI/EBV) compared to responders (MSS) (**Figure 4D**). These data are consistent with the
225 understanding that angiogenesis can be associated with immune suppression[47], suggesting
226 that a pro-angiogenic environment may impede ICB response in gastric cancer. In urothelial
227 cancer we found that cancer DEGs were enriched for neuron-related functional terms
228 (**Figure 4E**), with neuronal genes overexpressed in ICB responders compared to ICB non-
229 responders (**Figure 4F**). This observation is concordant with a previous study linking the
230 neuronal expression subtype[48] of urothelial cancer with poor overall survival but high
231 response rate to ICB[49].

232 Overall, while these results indicate an overall paucity of tissue-agnostic cancer-cell-
233 intrinsic features of ICB response, they also highlight the potential for tissue and tumor-type
234 specific expression signatures in cancer cells that may predict ICB response.

235

236 **Lack of cancer intrinsic immune checkpoint regulation across cancer types**

237 To further investigate if specific ligand-receptor interactions between cancer and immune
238 cells may promote primary ICB resistance, we systematically investigated the expression of
239 30 known immune checkpoint ligand-receptor pairs in both the cancer and stromal
240 components of the TME (**Figure 5A**). We found stromal overexpression of 13 checkpoint
241 receptors and 2 checkpoint ligands to be associated with ICB response across cancer types.
242 Checkpoint ligands PD-L1 and PD-L2 and their receptor PD-1 were coordinately upregulated
243 in the stroma of ICB responders compared to ICB non-responders. PD-L1 (*CD274*) and PD-1

244 were significantly upregulated in the stroma of ICB responders in 6 out of 7 cohorts studied
245 (p-value<0.05, permutation test), while PD-L2 was upregulated in 5 out of the 7 cohorts
246 (**Supplementary Figure 6).** Interestingly, no checkpoint ligands were consistently
247 differentially expressed and associated with ICB response in cancer cells across tumor types.
248 In addition to immune checkpoints, cytokines also play important roles in tumor
249 immunity[50-52]. We examined the expression of 13 pairs of cytokines and cytokine receptors
250 known to be involved in tumor immunity[50,52], aiming to identify cytokine signals associated
251 with ICB response (**Figure 5B**). Similar to our analysis for immune checkpoints, we found
252 that cancer-intrinsic cytokine expression was not associated with ICB response across tumor
253 types. However, six cytokines (*IFNG*, *FASLG*, *CXCL13*, *CCL5*, *CXCL10* and *CXCL9*), and the
254 corresponding receptors for three of the cytokines (*CCR5* for *CCL5*, *CXCR3* for *CXCL9* and
255 *CXCL10*) were significantly upregulated in the stroma of ICB responders, consistent with
256 previous observations[11,25]. Overall, our analysis finds no evidence for a universal mechanism
257 by which cancer cells inhibit immune cells via checkpoints interactions or
258 chemokine/cytokine signaling.
259

260 **A 3-feature classifier robustly predicts ICB response across cancer types**

261 Next, we explored if we could build an accurate predictor of ICB response based on the
262 consensus DEGs identified earlier (**Figure 6A**). We focused on the 59 stroma-specific DEGs
263 (**Figure 2A**) as they were more consistent across tumor types, in comparison to cancer DEGs,
264 and therefore more likely to be generalize to unseen cancer types. While a stroma
265 transcriptomic signature would likely reflect the state and favorability of the tumor
266 microenvironment for ICB response, TMB is likely a proxy of the tumor immunogenicity.
267 Since the stroma DEGs and TMB likely represent different facets of tumor immunity, we

268 hypothesized that these could be orthogonal predictors of ICB response and therefore
269 considered both factors for the predictive model. To identify the best predictive features of
270 ICB response, we used LASSO logistic regression with 10-fold cross-validation to select
271 robust features from the set of 59 stromal DEGs and TMB (**Figure 6A**). The final model was
272 built using the top-3 features: TMB, *IFNG* expression, and *FCER1A* expression (**Figure 6B**).
273 The model was trained on 461 samples from the ICB discovery cohorts with both
274 transcriptomic and genomic data. Next, we evaluated the model performance on 2
275 independent test cohorts. Test cohort 1 consisted of 49 tumors from melanoma patients
276 treated with the PD-L1 inhibitor nivolumab[53]. Test cohort 2 consisted of 87 tumors from 20
277 solid cancer types treated with a mix of ICB agents[54]. We calculated the area under the
278 receiver operating curve (AUC) of our model, and benchmarked it against established
279 biomarkers of ICB response, namely CXCL9+TMB[14], T-cell GEP[11], TIDE[13,55], TMB alone[2,8], and
280 PD-L1 expression[3]. Intriguingly, our compact 3-feature predictor outperformed all existing
281 biomarkers. On test cohort 1, the 3-feature model achieved an AUC of 0.66, compared to
282 0.62 for CXCL9+TMB, 0.64 for T-cell GEP, 0.44 for TIDE, 0.55 for PD-L1 expression, and 0.57
283 for the TMB-only model. On test cohort 2, the model achieved an AUC of 0.72, compared to
284 0.67 for CXCL9+TMB, 0.63 for T-cell GEP, 0.32 for TIDE, 0.61 for PD-L1 expression, and 0.55
285 for the TMB-only model (**Figure 6C**). This demonstrates that *FCER1A,* a novel negative
286 biomarker of ICB response identified from our transcriptome-wide analysis, contributes
287 additional predictive power of ICB response over existing biomarkers. Furthermore, in
288 cohorts that included survival data, model predictions were significantly associated with
289 progression free survival (**Figure 6D**) and, to a lesser extent, overall survival (**Supplementary**
290 **Figure 7**).
291

292 **Discussion**

293 In this study, we performed a transcriptome-wide meta-analysis of ICB response in 1486
294 tumors. These tumor samples included 534 tumors with annotated clinical response to ICB
295 treatment, and 952 tumors from cancer types enriched for MSI and ICB-responding tumors.
296 Using *in silico* tumor transcriptome deconvolution, we analyzed gene expression signatures
297 of cancer and stromal cells and identified differentially expressed genes associated with ICB
298 response across tumor types. Strikingly, this meta-analysis revealed a paucity of ICB-
299 response DEGs in cancer cells as compared to stromal cells. The few cancer DEGs that we
300 identified by the meta-analysis were more likely related to the biology of MSI tumors and
301 their DNA mismatch repair deficiency rather than being general determinants of ICB
302 response. In contrast, our analysis revealed 59 stroma-specific ICB-response DEGs, which
303 were strongly enriched in immune-related pathways and processes (**Figure 7**).

304 The two chemokine ligands, *CXCL9* and *CXCL13*, constituted the top-2 stromal genes
305 overexpressed in ICB responders. Underlining the validity of our approach, these two genes
306 have been highlighted for their roles in anti-tumor immunity and association with favorable
307 ICB response in multiple recent studies[14,31,32]. Previous studies suggest CXCL13 may play
308 dual roles in ICB response. First, CXCL13 is produced by Tfh cells and involved in B-cell
309 organization in TLS [29], and the presence of TLS can be a positive predictor of ICB
310 response[30,44]. Second, *CXCL13* has been reported to be highly expressed by neo-antigen
311 reactive CD8+ T-cells directly involved in cancer cell killing [56,57]. In line with these findings,
312 we found enrichment of both Tfh and CD8+ T-cells in tumors of ICB responders compared to
313 non-responders across cancer types (**Figure 3,7**). Additionally, the abundance of these two
314 cell types correlates with *CXCL13* expression. In agreement with recent work, we found that
315 *CXCL9* expression is strongly correlated with M1 macrophage infiltration[31,58], and M1

316 macrophages were one of the most differentially enriched immune cell types in ICB
317 responders (**Figure 3a**). Although myeloid infiltration has traditionally been associated with
318 immune suppression[40], our data is consistent with the hypothesis that M1 macrophage
319 infiltration, and macrophage polarization, could be an important determinant of tumor
320 sensitivity to ICB.

321 Intriguingly, we also identified a set of immune-related genes that were negatively
322 associated with ICB response. Among these genes, *FCER1A* and *CH25H* have previously been
323 reported to be over-expressed in anti-inflammatory M2 macrophages[35,59], and FCER1A+
324 TAMs have been reported to promote tumor progression by engaging in a positive feedback
325 loop with tumor initiating cells[36].

326 Interestingly, we observed an enrichment of the resting states of CD4 memory T-
327 cells, dendritic cells and mast cells in ICB non-responders. In contrast, the activated states of
328 these cell types are enriched in the tumors of ICB responders (**Figure 3B**). Furthermore,
329 while *FCER1A* is expressed in antigen presenting cells like dendritic cells and macrophages,
330 we noted that its expression is 25 times higher in resting dendritic cells compared to
331 activated dendritic cells, and 14 times higher in M2 macrophages compared to M1
332 macrophages[39]. These results suggest that a pre-existing immunosuppressive
333 microenvironment, associated with resting immune cells and high *FCER1A* expression, may
334 prevent effective anti-tumor immune responses in ICB non-responders.

335 Analyses of immune checkpoint and cytokine ligand-receptor interactions revealed
336 coordinated upregulation of several ligand-receptor pairs in the stroma of tumors from ICB
337 responders, including genes encoding PD-L1/PD-L2 and their receptor PD-1, CXCL9/CXCL10
338 and their receptor CXCR3, and CCL5 and its receptor CCR5 (**Figure 5, Figure 7**). In contrast,
339 we did not find consistent expression changes of checkpoint proteins and cytokines in

340 cancer cells of ICB responders. Among chemokines upregulated in ICB responders, CXCL9,
341 CXCL10, and CXCL13 promote lymphocyte recruitment, while CCL5 is a chemoattractant of
342 myeloid cells. CCL5 recruits CCR5+ blood monocytes and neutrophils that can differentiate
343 into immunosuppressive tumor associated macrophages and neutrophils[50,51]. In addition,
344 CCL5 also has direct pro-tumoral effects on cancer cells, promoting cancer proliferation and
345 metastasis[50,51]. Preclinical and clinical studies suggested that targeting the CCL5-CCR5 axis
346 could enhance anti-tumoral response[60,61]. As *CCL5* and *CCR5* are both overexpressed in ICB
347 responders, our result suggests that targeting CCL5-CCR5 signaling in conjunction with ICB
348 might further potentiate anti-tumoral immune response. Currently, the majority of
349 companion diagnostics for PD-1/PD-L1 inhibitors measure PD-L1 expression level on either
350 cancer cells alone, or on both cancer cells and infiltrating immune cells, but seldomly on
351 immune cells only[16,62]. Our study strongly suggests that PD-L1 expression on immune cells is
352 a more consistent determinant of ICB response across tumor types.

353 Using the stromal consensus DEGs identified from the meta-analysis, we developed
354 a model to predict ICB response from gene expression data and TMB. This 3-feature model
355 comprised of a single positive marker of immune infiltration (*IFNG*), a single negative marker
356 of immune suppression (*FCER1A*), in combination with TMB. The model robustly predicted
357 ICB response across both the discovery cohort and 2 independent test cohorts,
358 outperforming existing gene expression signatures for ICB response. While ideal pan-cancer
359 biomarkers of ICB response should be robust across patient cohorts, we noticed that the Liu
360 et al. melanoma cohort did not share many DEGs with the other cohorts, including other
361 melanoma cohorts. This result highlights significant heterogeneity between ICB cohorts,
362 even among cohorts of the same tumor type. It is unclear to what extent this heterogeneity
363 arise from patient selection, differences in ICB regime, differences in prior treatments,

364 different sample collection protocols, or differences in gene expression assays. This
365 highlights the need for large, consistently selected patient cohorts, with standardized gene
366 expression profiling to further improve biomarker discovery.

367 As cancer cells are under negative selective pressure from the immune system,
368 several mechanisms of immune escape by cancer cells have been proposed: (i) cancer cells
369 down-regulate antigen presentation by deleting HLA alleles[46], (ii) cancer cells deplete
370 neoantigens to avoid detection[63], (iii) oncogenic signaling may up-regulate PD-L1 expression
371 and suppress T-cell recruitment[64]. However, the prevalence of these immune evasion
372 mechanisms are still unclear. A recent meta-analysis found no association between loss of
373 heterozygosity of HLA alleles and ICB response across ICB cohorts[14]. Furthermore, a pan-
374 cancer analysis failed to detect neo-antigen depletion signals in most tumor types[65].
375 Similarly, we found a lack of conserved cancer-intrinsic mechanisms of immune evasion on
376 the transcriptomic level, which challenge the prevailing dogma that cancer cell-intrinsic
377 expression of checkpoint ligands can modulate immune activity and predict ICB response
378 across cancer types. These insights have profound implications on biomarker assays and *in*
379 *vitro* model systems for development of improved ICB drugs. These results suggest that
380 cancer cells adopt diverse mechanisms of immune evasion, with no universal strategy
381 adopted by cancer cells to avoid immune-mediated killing. The growing number of
382 molecularly characterized ICB cohorts will enable further exploration of the importance and
383 prevalence of the different cancer-intrinsic immune evasion strategies in determining ICB
384 response.
385
386

387 **Methods**

388 **Clinical cohorts treated with ICB**

389 Data from the following studies were used for discovery:

390 1. Kim et al.[22] cohort comprises of 45 metastatic gastric cancer patients treated with
391 PD-1 inhibitor pembrolizumab
392 2. Mariathasan et al.[23] cohort comprises of 298 metastatic urothelial cancer patients
393 treated with PD-L1 inhibitor atezolizumab
394 3. Liu et al. [25] comprises of 118 metastatic melanoma patients treated with PD-1
395 inhibitors nivolumab or pembrolizumab
396 4. Gide et al. [24] comprises of 73 metastatic melanoma patients treated with anti-PD-1
397 alone (nivolumab or pembrolizumab, or with anti-CTLA-4 (nivolumab or
398 pembrolizumab with ipilimumab)

399 Data from the following studies were used for validation:

400 1. Riaz et al. [53] comprises 49 advanced melanoma patients treated with PD-L1 inhibitor
401 nivolumab.
402 2. Pender et al.[54] comprises of 87 metastatic tumors from 20 solid cancer types treated
403 with a mix of ICB agents.

404

405 **Gene expression data collection and normalization**

406 Expression data of TCGA colorectal (COAD, READ), gastric (STAD) and endometrial (UCEC)
407 tumors were downloaded from the UCSC Xena repository. Raw genomic and transcriptomic
408 data of Kim et al.[22] gastric ICB cohort were downloaded from the European Nucleotide
409 Archive, and processed using the bcbio nextgen pipeline. Briefly, RNAseq reads were aligned
410 to the human transcriptome using STAR[66], and TPM counts were quantified using SALMON[67].

411 Processed transcriptomic data of Mariathasan et al. (urothelial)[23], Liu et al. (melanoma)[25],
412 Gide et al. (melanoma)[24], Riaz et al. (melanoma)[53], and Pender et al. (mixed)[54] ICB cohorts
413 were obtained from the original publications. Genes with 0 expression in more than 50% of
414 the samples were removed. All gene expression data were log2 transformed and upper
415 quantile normalized across all cohorts.
416
417 **Tumor purity estimation**
418 Purity estimates of TCGA tumors were obtained from a previous publication[20], where
419 consensus purity was estimated from mutation allele frequencies, copy number variations
420 and RNA profiles of each tumor. Tumor purity of samples from ICB cohorts were estimated
421 using PUREE[68], a machine learning method for tumor purity estimation from bulk RNA
422 transcriptomics. For the Kim et al. gastric ICB cohort[49] where genomic data is also available,
423 we calculated consensus purity estimates based on both genomic and transcriptomic data.
424 We first computed purity estimates using 2 RNA-based methods (PUREE[68] and Estimate[69]),
425 and 2 DNA-based methods (Sequenza[70], PurBayes[71]). Then, we performed quantile-quantile
426 normalization on the purity estimates of individual methods, and took the mean normalized
427 purity estimate as the consensus purity.
428
429 **MSI status and ICB response classification**
430 MSI status of TCGA tumors were obtained from two previous pan-cancer studies of
431 microsatellite instability[9,10]. EBV status of the TCGA STAD tumors was obtained from a
432 previous TCGA study on gastrointestinal cancers[72].Clinical annotations of ICB response
433 based on the RECIST criteria were obtained from the original studies. Consistent with recent
434 literature[14,23], we classified “CR/PR” as responders and “SD/PD” as non-responders.

435

436 **Expression deconvolution**

437 We modelled bulk tumor expression as the sum of cancer and stroma expression, weighted

438 by cancer purity[20]. This can be written as,

439

$$y_j = c_j p + s_j(1 - p) + \varepsilon_j$$

440 where y_j is a *n* x 1 vector of bulk tumor expression for gene *j* in *n* samples, c_j and s_j are the

441 average cancer- and stroma-specific expression for a gene *j*, p is *n* x 1 vector of cancer purity,

442 and ε_j is the residual. Given bulk expression (y_j) and tumor purity (p), non-negative least

443 squares (NNLS) regression can be used to estimate cancer- (c_j) and stroma-specific (s_j)

444 expression for each gene. c_j and s_j represent estimates of mean cancer- and stroma-specific

445 expression for a gene j for $p_c = 1$ and $p_s = 0$, respectively. The standard error of these

446 predicted values for gene *j* is calculated as,

447

$$SE_{j,h} = \sqrt{MSE + \left(1 + \frac{1}{n} + \frac{(p_h - \bar{p})^2}{\sum(p_i - \bar{p})^2}\right)}$$

448

449 where $p_h = p_c = 1$ for cancer-specific expression and $p_h = p_s = 0$ for stroma-specific

450 expression; MSE is the mean square error.

451

452 **Permutation statistic to identify differentially expressed genes**

453 To test differences in cancer (or stroma) expression between two response groups (e.g.

454 $c_{Rj} - c_{NRj}$ for gene *j*), the above approach is applied to each group separately, and a test

455 statistic is calculated as,

456

$$Z_{obs,j}^2 = \left(\frac{c_{Rj} - c_{NRj}}{\sqrt{SE_{Rj}^2 + SE_{NRj}^2}} \right)^2$$

457

458 To assess significance under the null hypothesis of no difference in cancer (stroma)
459 expression between the 2 response groups, a null distribution is generated by permutation,
460 where group labels are first randomly shuffled 10,000 times and the above procedure is
461 applied to each permuted dataset, generating a null distribution of Z_{perm}^2 statistics. A p-
462 value is calculated as,

463

$$p = P\left(Z_{perm}^2 \geq Z_{obs}^2\right)$$

464

465 That is, the probability of observing Z_{obs}^2 or larger, given the null hypothesis is true.

466

467 **Identification of consensus DEGs across cancer types**

468 For each gene and each tumor compartment (caner or stroma), a meta p-value is computed
469 by combining the permutation p-values of all cancer cohorts using Fisher's method. We
470 used the Bonferroni correction to adjust for multiple testing to maintain the overall α at
471 0.01. Genes that are differentially expressed in different directions in at least 2 cohorts were
472 removed. Finally, to eliminate DEGs that are involved in MSI biology but are not directly
473 associated with ICB response, we require the final list of consensus DEGs to be differentially
474 expressed in at least 1 ICB cohort (nominal p-value<0.1).

475

476 **Pathway enrichment analysis**

477 To find out if the DEGs identified are enriched in specific biological processes, pathway
478 enrichment analysis was performed using ClueGo[73] with default parameters. Briefly, two-
479 sided-hypergeometric statistic was used to compute the enrichment of a given list of DEGs
480 in GO biological processes terms, and the resulting p-values were corrected for multiple
481 testing using the Bonferroni step down approach. To aid interpretation, significant biological
482 terms with high overlap as measured by the kappa coefficient were merged into functional
483 groups. To calculate the enrichment of stroma DEGs in immune-related functions, we
484 defined immune-related genes as genes in the "immune system process" term and its child
485 terms in the GO biological processes dataset. Additionally, we manually curated stroma
486 DEGs not labeled as immune genes by GO, and further labeled *FCER1A*, *GZMH*, *FCRL6*, *SIRPG*,
487 *JAKMIP1*, and *WARS* as immune-related genes based on literature search.

488

489 **Building a predictive model of ICB response**

490 We used 461 patients from 3 discover cohorts (Mariathasan et al[23], Liu et al[25], Kim et al.[22])
491 with both transcriptomic data and TMB as training data. TMB was obtained from the
492 original publications and standardized into Z-scores (mean=0, standard deviation=1). To
493 identify the most predictive features of ICB response, we used the least absolute shrinkage
494 and selection operator (LASSO) to select features from the 59 stroma DEGs identified earlier
495 and TMB. LASSO penalizes the sum of the absolute values of the regression coefficients,
496 shrinking some coefficients to zero, and thereby identifies a simpler and more interpretable
497 model. The regularization parameter λ was chosen by 10-fold cross-validation such that the
498 error of the selected model was within 1 standard deviation from the minimum error.
499 LASSO regression and cross validation were performed using the 'glmnet' package in R. To

500 select for the most robust features, we bootstrapped 100 samples with 90% of the data in
501 each bootstrap, and selected features that are found by at least 75% of the bootstraps for
502 the final model. The final logistic regression model is built on all 461 training samples using
503 the features selected by LASSO (TMB+IFNG+FCER1A).
504
505 **Benchmarking ICB prediction model against existing biomarkers**
506 T-cell GEP scores were calculated from normalized RNAseq data using the weights provided
507 by Ayers et al. 2018[11]. TIDE scores were calculated from normalized RNAseq data using the
508 TIDE web platform[55]. The CXCL-9+TMB model was trained on our training cohort using
509 logistic regression.
510
511 **Immune cell enrichment analysis**
512 Immune deconvolution was performed using CibersortX (with the LM22 signature matrix)[39]
513 to estimate the absolute abundance of immune cell subsets for each tumor. Immune cell
514 subsets that are differentially infiltrated between responders and non-responders were
515 identified using the Wilcoxon rank-sum test.
516
517 **Data and code availability**
518 The code used to generate figures in the manuscript is provided in **Supplementary Data 1**.
519
520 **Acknowledgements**
521 This study was supported by the Singapore Ministry of Health's National Medical Research
522 Council under its OF-IRG program (OFIRG18may-0075) and Singapore Agency for Science,

Technology and Research (A*STAR) under its Biomedical Engineering Programme (C221118001 and C221318004)

525 **References**

526 1. O'Reilly EM, Oh DY, Dhani N, et al. Durvalumab With or Without Tremelimumab for
527 Patients With Metastatic Pancreatic Ductal Adenocarcinoma: A Phase 2 Randomized Clinical
528 Trial. *JAMA Oncol*. Oct 1 2019;5(10):1431-1438. doi:10.1001/jamaoncol.2019.1588
529 2. Yarchoan M, Hopkins A, Jaffee EM. Tumor Mutational Burden and Response Rate to
530 PD-1 Inhibition. *N Engl J Med*. 12 21 2017;377(25):2500-2501. doi:10.1056/NEJMc1713444
531 3. Havel JJ, Chowell D, Chan TA. The evolving landscape of biomarkers for checkpoint
532 inhibitor immunotherapy. *Nat Rev Cancer*. 03 2019;19(3):133-150. doi:10.1038/s41568-019-
533 0116-x
534 4. Marcus L, Lemery SJ, Keegan P, Pazdur R. FDA Approval Summary: Pembrolizumab
535 for the Treatment of Microsatellite Instability-High Solid Tumors. *Clin Cancer Res*. 07 01
536 2019;25(13):3753-3758. doi:10.1158/1078-0432.CCR-18-4070
537 5. FDA approves pembrolizumab for adults and children with TMB-H solid tumors. June
538 17, 2020.
539 6. Banchereau R, Leng N, Zill O, et al. Molecular determinants of response to PD-L1
540 blockade across tumor types. *Nat Commun*. 06 25 2021;12(1):3969. doi:10.1038/s41467-
541 021-24112-w
542 7. Valero C, Lee M, Hoen D, et al. Response Rates to Anti-PD-1 Immunotherapy in
543 Microsatellite-Stable Solid Tumors With 10 or More Mutations per Megabase. *JAMA Oncol*.
544 May 01 2021;7(5):739-743. doi:10.1001/jamaoncol.2020.7684
545 8. Samstein RM, Lee CH, Shoushtari AN, et al. Tumor mutational load predicts survival
546 after immunotherapy across multiple cancer types. *Nat Genet*. 02 2019;51(2):202-206.
547 doi:10.1038/s41588-018-0312-8
548 9. Cortes-Ciriano I, Lee S, Park WY, Kim TM, Park PJ. A molecular portrait of
549 microsatellite instability across multiple cancers. *Nat Commun*. 06 06 2017;8:15180.
550 doi:10.1038/ncomms15180
551 10. Bonneville R, Krook MA, Kautto EA, et al. Landscape of Microsatellite Instability
552 Across 39 Cancer Types. *JCO Precis Oncol*. 2017;2017doi:10.1200/PO.17.00073
553 11. Ayers M, Lunceford J, Nebozhyn M, et al. IFN-γ-related mRNA profile predicts clinical
554 response to PD-1 blockade. *J Clin Invest*. Aug 01 2017;127(8):2930-2940.
555 doi:10.1172/JCI91190
556 12. Cristescu R, Mogg R, Ayers M, et al. Pan-tumor genomic biomarkers for PD-1
557 checkpoint blockade-based immunotherapy. *Science*. Oct 12
558 2018;362(6411)doi:10.1126/science.aar3593
559 13. Jiang P, Gu S, Pan D, et al. Signatures of T cell dysfunction and exclusion predict
560 cancer immunotherapy response. *Nat Med*. 10 2018;24(10):1550-1558.
561 doi:10.1038/s41591-018-0136-1
562 14. Litchfield K, Reading JL, Puttick C, et al. Meta-analysis of tumor- and T cell-intrinsic
563 mechanisms of sensitization to checkpoint inhibition. *Cell*. 02 04 2021;184(3):596-614.e14.
564 doi:10.1016/j.cell.2021.01.002
565 15. Bareche Y, Kelly D, Abbas-Aghababazadeh F, et al. Leveraging big data of immune
566 checkpoint blockade response identifies novel potential targets. *Ann Oncol*. Dec
567 2022;33(12):1304-1317. doi:10.1016/j.annonc.2022.08.084
568 16. Nishino M, Ramaiya NH, Hatabu H, Hodi FS. Monitoring immune-checkpoint
569 blockade: response evaluation and biomarker development. *Nat Rev Clin Oncol*. Nov
570 2017;14(11):655-668. doi:10.1038/nrclinonc.2017.88

571 17. Guruprasad P, Lee YG, Kim KH, Ruella M. The current landscape of single-cell
572 transcriptomics for cancer immunotherapy. *J Exp Med*. Jan 4
573 2021;218(1)doi:10.1084/jem.20201574
574 18. Gohil SH, Iorgulescu JB, Braun DA, Keskin DB, Livak KJ. Applying high-dimensional
575 single-cell technologies to the analysis of cancer immunotherapy. *Nat Rev Clin Oncol*. Apr
576 2021;18(4):244-256. doi:10.1038/s41571-020-00449-x
577 19. Zhong Y, Liu Z. Gene expression deconvolution in linear space. *Nat Methods*. Dec 28
578 2011;9(1):8-9; author reply 9. doi:10.1038/nmeth.1830
579 20. Ghoshdastider U, Rohatgi N, Mojtabavi Naeini M, et al. Pan-Cancer Analysis of
580 Ligand-Receptor Cross-talk in the Tumor Microenvironment. *Cancer Res*. 04 01
581 2021;81(7):1802-1812. doi:10.1158/0008-5472.CAN-20-2352
582 21. Rohatgi N, Ghoshdastider U, Baruah P, Kulshrestha T, Skanderup AJ. A pan-cancer
583 metabolic atlas of the tumor microenvironment. *Cell Rep*. May 10 2022;39(6):110800.
584 doi:10.1016/j.celrep.2022.110800
585 22. Kim ST, Cristescu R, Bass AJ, et al. Comprehensive molecular characterization of
586 clinical responses to PD-1 inhibition in metastatic gastric cancer. *Nat Med*. 09
587 2018;24(9):1449-1458. doi:10.1038/s41591-018-0101-z
588 23. Mariathasan S, Turley SJ, Nickles D, et al. TGFβ attenuates tumour response to PD-L1
589 blockade by contributing to exclusion of T cells. *Nature*. 02 22 2018;554(7693):544-548.
590 doi:10.1038/nature25501
591 24. Gide TN, Quek C, Menzies AM, et al. Distinct Immune Cell Populations Define
592 Response to Anti-PD-1 Monotherapy and Anti-PD-1/Anti-CTLA-4 Combined Therapy. *Cancer*
593 *Cell*. 02 11 2019;35(2):238-255.e6. doi:10.1016/j.ccell.2019.01.003
594 25. Liu D, Schilling B, Sucker A, et al. Integrative molecular and clinical modeling of
595 clinical outcomes to PD1 blockade in patients with metastatic melanoma. *Nat Med*. 12
596 2019;25(12):1916-1927. doi:10.1038/s41591-019-0654-5
597 26. Green AK, Feinberg J, Makker V. A Review of Immune Checkpoint Blockade Therapy
598 in Endometrial Cancer. *Am Soc Clin Oncol Educ Book*. Mar 2020;40:1-7.
599 doi:10.1200/EDBK_280503
600 27. Kubota Y, Kawazoe A, Sasaki A, et al. The Impact of Molecular Subtype on Efficacy of
601 Chemotherapy and Checkpoint Inhibition in Advanced Gastric Cancer. *Clin Cancer Res*. 07 15
602 2020;26(14):3784-3790. doi:10.1158/1078-0432.CCR-20-0075
603 28. Gorbachev AV, Kobayashi H, Kudo D, et al. CXC chemokine ligand 9/monokine
604 induced by IFN-gamma production by tumor cells is critical for T cell-mediated suppression
605 of cutaneous tumors. *J Immunol*. Feb 15 2007;178(4):2278-86.
606 doi:10.4049/jimmunol.178.4.2278
607 29. Kazanietz MG, Durando M, Cooke M. CXCL13 and Its Receptor CXCR5 in Cancer:
608 Inflammation, Immune Response, and Beyond. *Front Endocrinol (Lausanne)*. 2019;10:471.
609 doi:10.3389/fendo.2019.00471
610 30. Hollern DP, Xu N, Thennavan A, et al. B Cells and T Follicular Helper Cells Mediate
611 Response to Checkpoint Inhibitors in High Mutation Burden Mouse Models of Breast Cancer.
612 *Cell*. 11 14 2019;179(5):1191-1206.e21. doi:10.1016/j.cell.2019.10.028
613 31. Qu Y, Wen J, Thomas G, et al. Baseline Frequency of Inflammatory Cxcl9-Expressing
614 Tumor-Associated Macrophages Predicts Response to Avelumab Treatment. *Cell Rep*. 07 07
615 2020;32(1):107873. doi:10.1016/j.celrep.2020.107873

616 32. Goswami S, Chen Y, Anandhan S, et al. mutation plus CXCL13 expression act as
617 combinatorial biomarkers to predict responses to immune checkpoint therapy in mUCC. *Sci*
618 *Transl Med*. 06 17 2020;12(548)doi:10.1126/scitranslmed.abc4220
619 33. Rooney MS, Shukla SA, Wu CJ, Getz G, Hacohen N. Molecular and genetic properties
620 of tumors associated with local immune cytolytic activity. *Cell*. Jan 15 2015;160(1-2):48-61.
621 doi:10.1016/j.cell.2014.12.033
622 34. Fehrenbacher L, Spira A, Ballinger M, et al. Atezolizumab versus docetaxel for
623 patients with previously treated non-small-cell lung cancer (POPLAR): a multicentre, open-
624 label, phase 2 randomised controlled trial. *Lancet*. Apr 30 2016;387(10030):1837-46.
625 doi:10.1016/S0140-6736(16)00587-0
626 35. Pellizzari G, Hoskin C, Crescioli S, et al. IgE re-programs alternatively-activated
627 human macrophages towards pro-inflammatory anti-tumoural states. *EBioMedicine*. May
628 2019;43:67-81. doi:10.1016/j.ebiom.2019.03.080
629 36. Taniguchi S, Elhance A, Van Duzer A, Kumar S, Leitenberger JJ, Oshimori N. Tumor-
630 initiating cells establish an IL-33-TGF-β niche signaling loop to promote cancer progression.
631 *Science*. 07 17 2020;369(6501)doi:10.1126/science.aay1813
632 37. Cyster JG, Dang EV, Reboldi A, Yi T. 25-Hydroxycholesterols in innate and adaptive
633 immunity. *Nat Rev Immunol*. Nov 2014;14(11):731-43. doi:10.1038/nri3755
634 38. Vollmar AM. The role of atrial natriuretic peptide in the immune system. *Peptides*.
635 Jun 2005;26(6):1086-94. doi:10.1016/j.peptides.2004.08.034
636 39. Newman AM, Steen CB, Liu CL, et al. Determining cell type abundance and
637 expression from bulk tissues with digital cytometry. *Nat Biotechnol*. 07 2019;37(7):773-782.
638 doi:10.1038/s41587-019-0114-2
639 40. Duan Z, Luo Y. Targeting macrophages in cancer immunotherapy. *Signal Transduct*
640 *Target Ther*. 03 26 2021;6(1):127. doi:10.1038/s41392-021-00506-6
641 41. Zeng D, Ye Z, Wu J, et al. Macrophage correlates with immunophenotype and
642 predicts anti-PD-L1 response of urothelial cancer. *Theranostics*. 2020;10(15):7002-7014.
643 doi:10.7150/thno.46176
644 42. Crotty S. T Follicular Helper Cell Biology: A Decade of Discovery and Diseases.
645 *Immunity*. 05 21 2019;50(5):1132-1148. doi:10.1016/j.immuni.2019.04.011
646 43. Garaud S, Buisseret L, Solinas C, et al. Tumor infiltrating B-cells signal functional
647 humoral immune responses in breast cancer. *JCI Insight*. 08 13
648 2019;5doi:10.1172/jci.insight.129641
649 44. Cui C, Wang J, Fagerberg E, et al. Neoantigen-driven B cell and CD4 T follicular helper
650 cell collaboration promotes anti-tumor CD8 T cell responses. *Cell*. 12 09 2021;184(25):6101-
651 6118.e13. doi:10.1016/j.cell.2021.11.007
652 45. Bindea G, Mlecnik B, Tosolini M, et al. Spatiotemporal dynamics of intratumoral
653 immune cells reveal the immune landscape in human cancer. *Immunity*. Oct 17
654 2013;39(4):782-95. doi:10.1016/j.immuni.2013.10.003
655 46. Kalbasi A, Ribas A. Tumour-intrinsic resistance to immune checkpoint blockade. *Nat*
656 *Rev Immunol*. Jan 2020;20(1):25-39. doi:10.1038/s41577-019-0218-4
657 47. Motz GT, Coukos G. The parallel lives of angiogenesis and immunosuppression:
658 cancer and other tales. *Nat Rev Immunol*. 09 23 2011;11(10):702-11. doi:10.1038/nri3064
659 48. Robertson AG, Kim J, Al-Ahmadie H, et al. Comprehensive Molecular
660 Characterization of Muscle-Invasive Bladder Cancer. *Cell*. 08 09 2018;174(4):1033.
661 doi:10.1016/j.cell.2018.07.036

662 49. Kim J, Kwiatkowski D, McConkey DJ, et al. The Cancer Genome Atlas Expression
663 Subtypes Stratify Response to Checkpoint Inhibition in Advanced Urothelial Cancer and
664 Identify a Subset of Patients with High Survival Probability. *Eur Urol*. 06 2019;75(6):961-964.
665 doi:10.1016/j.eururo.2019.02.017
666 50. Nagarsheth N, Wicha MS, Zou W. Chemokines in the cancer microenvironment and
667 their relevance in cancer immunotherapy. *Nat Rev Immunol*. Sep 2017;17(9):559-572.
668 doi:10.1038/nri.2017.49
669 51. Mollica Poeta V, Massara M, Capucetti A, Bonecchi R. Chemokines and Chemokine
670 Receptors: New Targets for Cancer Immunotherapy. *Front Immunol*. 2019;10:379.
671 doi:10.3389/fimmu.2019.00379
672 52. Dranoff G. Cytokines in cancer pathogenesis and cancer therapy. *Nat Rev Cancer*. Jan
673 2004;4(1):11-22. doi:10.1038/nrc1252
674 53. Riaz N, Havel JJ, Makarov V, et al. Tumor and Microenvironment Evolution during
675 Immunotherapy with Nivolumab. *Cell*. Nov 02 2017;171(4):934-949.e16.
676 doi:10.1016/j.cell.2017.09.028
677 54. Pender A, Titmuss E, Pleasance ED, et al. Genome and Transcriptome Biomarkers of
678 Response to Immune Checkpoint Inhibitors in Advanced Solid Tumors. *Clin Cancer Res*. 01
679 01 2021;27(1):202-212. doi:10.1158/1078-0432.CCR-20-1163
680 55. Fu J, Li K, Zhang W, et al. Large-scale public data reuse to model immunotherapy
681 response and resistance. *Genome Med*. Feb 26 2020;12(1):21. doi:10.1186/s13073-020-
682 0721-z
683 56. Zheng C, Fass JN, Shih YP, et al. Transcriptomic profiles of neoantigen-reactive T cells
684 in human gastrointestinal cancers. *Cancer Cell*. 04 11 2022;40(4):410-423.e7.
685 doi:10.1016/j.ccell.2022.03.005
686 57. Lowery FJ, Krishna S, Yossef R, et al. Molecular signatures of antitumor neoantigen-
687 reactive T cells from metastatic human cancers. *Science*. 02 25 2022;375(6583):877-884.
688 doi:10.1126/science.abl5447
689 58. House IG, Savas P, Lai J, et al. Macrophage-Derived CXCL9 and CXCL10 Are Required
690 for Antitumor Immune Responses Following Immune Checkpoint Blockade. *Clin Cancer Res*.
691 01 15 2020;26(2):487-504. doi:10.1158/1078-0432.CCR-19-1868
692 59. Preuss I, Ludwig MG, Baumgarten B, et al. Transcriptional regulation and functional
693 characterization of the oxysterol/EBI2 system in primary human macrophages. *Biochem*
694 *Biophys Res Commun*. Apr 11 2014;446(3):663-8. doi:10.1016/j.bbrc.2014.01.069
695 60. Halama N, Zoernig I, Berthel A, et al. Tumoral Immune Cell Exploitation in Colorectal
696 Cancer Metastases Can Be Targeted Effectively by Anti-CCR5 Therapy in Cancer Patients.
697 *Cancer Cell*. Apr 11 2016;29(4):587-601. doi:10.1016/j.ccell.2016.03.005
698 61. Ban Y, Mai J, Li X, et al. Targeting Autocrine CCL5-CCR5 Axis Reprograms
699 Immunosuppressive Myeloid Cells and Reinvigorates Antitumor Immunity. *Cancer Res*. 06 01
700 2017;77(11):2857-2868. doi:10.1158/0008-5472.CAN-16-2913
701 62. Twomey JD, Zhang B. Cancer Immunotherapy Update: FDA-Approved Checkpoint
702 Inhibitors and Companion Diagnostics. *AAPS J*. Mar 7 2021;23(2):39. doi:10.1208/s12248-
703 021-00574-0
704 63. Zapata L, Caravagna G, Williams MJ, et al. Immune selection determines tumor
705 antigenicity and influences response to checkpoint inhibitors. *Nat Genet*. Mar
706 2023;55(3):451-460. doi:10.1038/s41588-023-01313-1
707 64. Spranger S, Gajewski TF. Impact of oncogenic pathways on evasion of antitumour
708 immune responses. *Nat Rev Cancer*. Mar 2018;18(3):139-147. doi:10.1038/nrc.2017.117

709 65. Van den Eynden J, Jimenez-Sanchez A, Miller ML, Larsson E. Lack of detectable
710 neoantigen depletion signals in the untreated cancer genome. *Nat Genet*. Dec
711 2019;51(12):1741-1748. doi:10.1038/s41588-019-0532-6
712 66. Dobin A, Davis CA, Schlesinger F, et al. STAR: ultrafast universal RNA-seq aligner.
713 *Bioinformatics*. Jan 01 2013;29(1):15-21. doi:10.1093/bioinformatics/bts635
714 67. Patro R, Duggal G, Love MI, Irizarry RA, Kingsford C. Salmon provides fast and bias-
715 aware quantification of transcript expression. *Nat Methods*. Apr 2017;14(4):417-419.
716 doi:10.1038/nmeth.4197
717 68. Revkov E, Kulshrestha T, Sung KW-K, Skanderup AJ. Accurate pan-cancer tumor
718 purity estimation from gene
719 expression data. 2022;doi: https://doi.org/10.1101/2022.06.01.494462
720 69. Yoshihara K, Shahmoradgoli M, Martínez E, et al. Inferring tumour purity and stromal
721 and immune cell admixture from expression data. *Nat Commun*. 2013;4:2612.
722 doi:10.1038/ncomms3612
723 70. Favero F, Joshi T, Marquard AM, et al. Sequenza: allele-specific copy number and
724 mutation profiles from tumor sequencing data. *Ann Oncol*. Jan 2015;26(1):64-70.
725 doi:10.1093/annonc/mdu479
726 71. Larson NB, Fridley BL. PurBayes: estimating tumor cellularity and subclonality in
727 next-generation sequencing data. *Bioinformatics*. Aug 01 2013;29(15):1888-9.
728 doi:10.1093/bioinformatics/btt293
729 72. Liu Y, Sethi NS, Hinoue T, et al. Comparative Molecular Analysis of Gastrointestinal
730 Adenocarcinomas. *Cancer Cell*. 04 09 2018;33(4):721-735.e8.
731 doi:10.1016/j.ccell.2018.03.010
732 73. Bindea G, Mlecnik B, Hackl H, et al. ClueGO: a Cytoscape plug-in to decipher
733 functionally grouped gene ontology and pathway annotation networks. *Bioinformatics*. Apr
734 15 2009;25(8):1091-3. doi:10.1093/bioinformatics/btp101
735

736

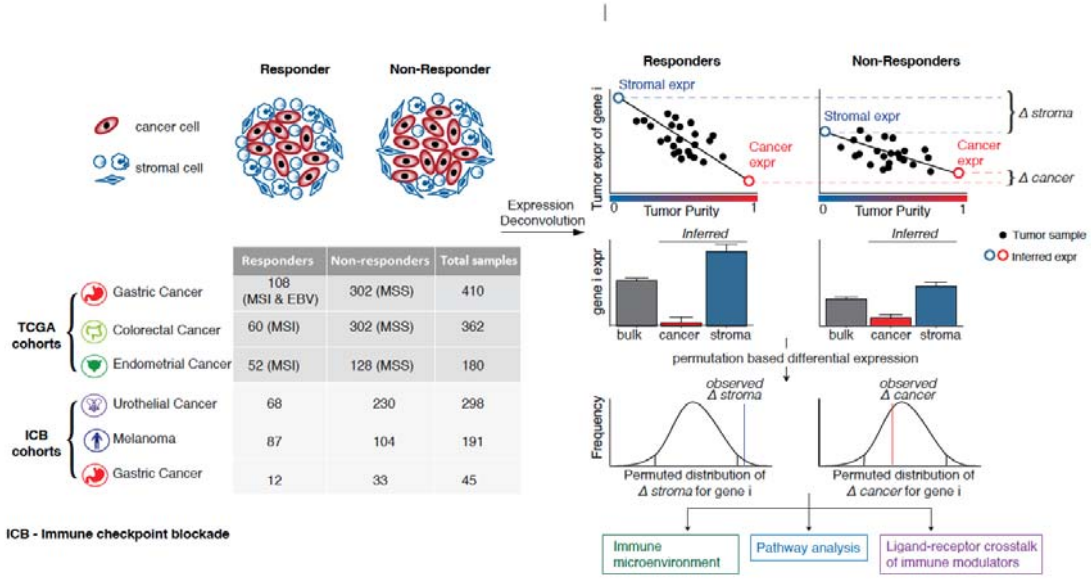

		Responders	Non-responders	Total samples
TCGA cohorts	Gastric Cancer	108 (MSI & EBV)	302 (MSS)	410
	Colorectal Cancer	60 (MSI)	302 (MSS)	362
	Endometrial Cancer	52 (MSI)	128 (MSS)	180
ICB cohorts	Urothelial Cancer	68	230	298
	Melanoma	87	104	191
	Gastric Cancer	12	33	45

Figure 1. Data summary and schematic of workflow for the analysis of determinants of immunotherapy response.

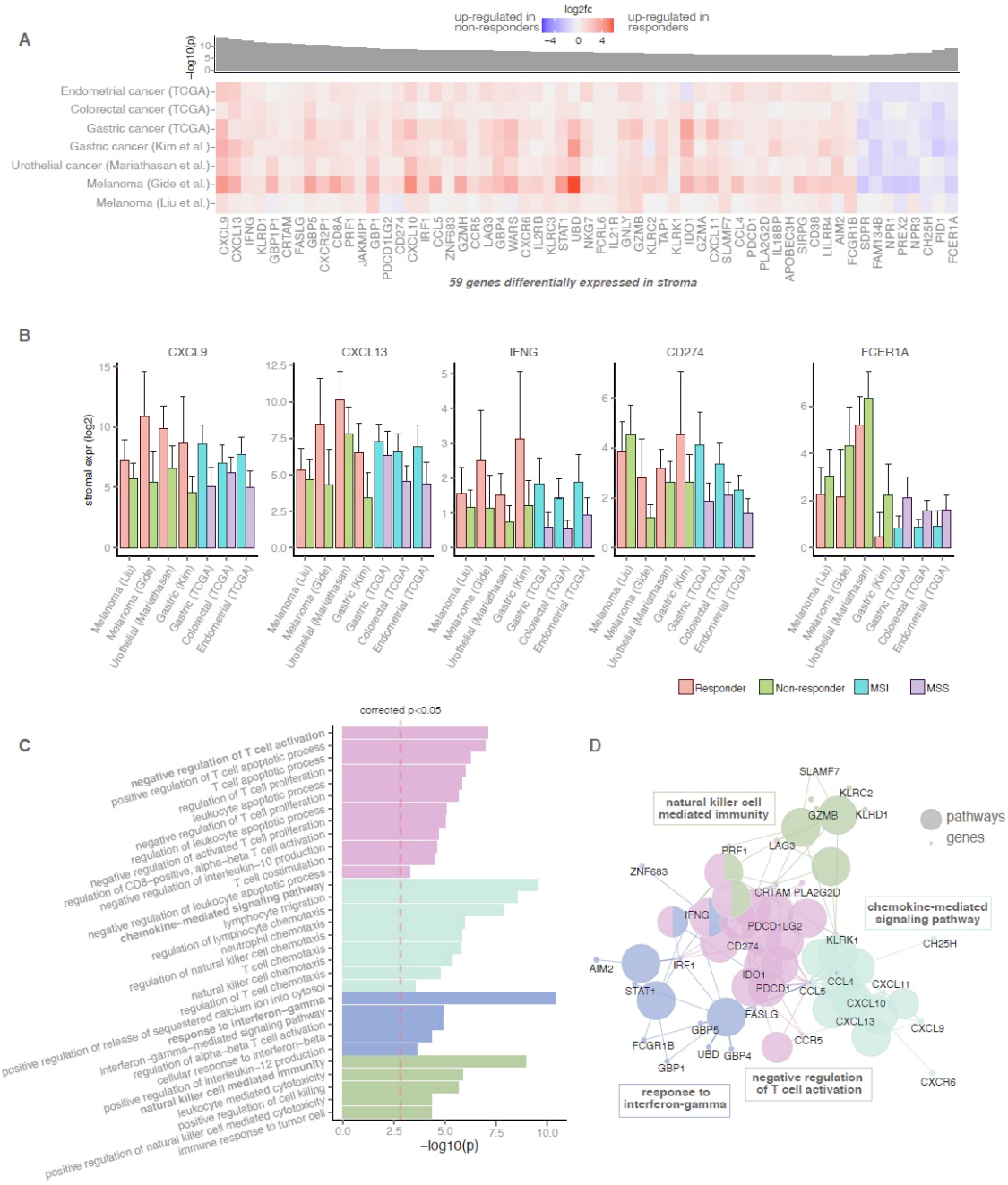

Figure 2. **Differentially expressed genes and pathways between responders and non-responders in the stroma. (A)** Heatmap of genes consistently differentially expressed across discovery cohorts in the stroma. Heatmaps are colored by the log2 fold change of gene expression. *P*-values of individual cohorts are combined using the Fisher's method, and the -log10(meta p-value) is presented in the bar plot. Genes with q-value<0.01 and *p*-value<0.1 at least 1 ICB cohort are shown. **(B)** Bar plots of deconvoluted stromal expression of the top differentially expressed genes. Error bars represent estimated standard error. **(C)** Pathway enrichment of differentially expressed genes in the stroma. Bar plot shows the -log10(p-value) of significantly enriched pathways. Similar pathways are grouped by color. (D)

Network representation of enriched pathways. Large nodes represent enriched pathways. Pathways with high similarity are fused and shown in the same color. Small nodes represent genes associated with each pathway.

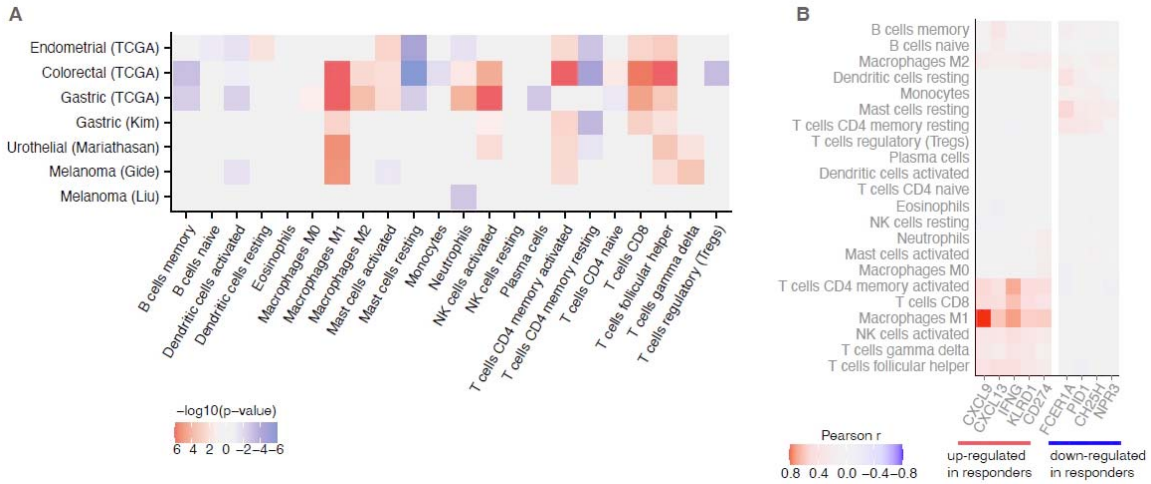

Figure 3. **Immune cell type enrichment analysis.** Abundance of immune cell types of each tumor is estimated using Cibersortx. **(A)** Heatmap of cell types analyzed. Heatmap is colored by the signed -log10(p-value) of the difference in Cibersortx scores between responders (MSI) and non-responders (MSS). **(B)** Correlations between the abundance of immune cell types with the gene expression of top stromal biomarkers.

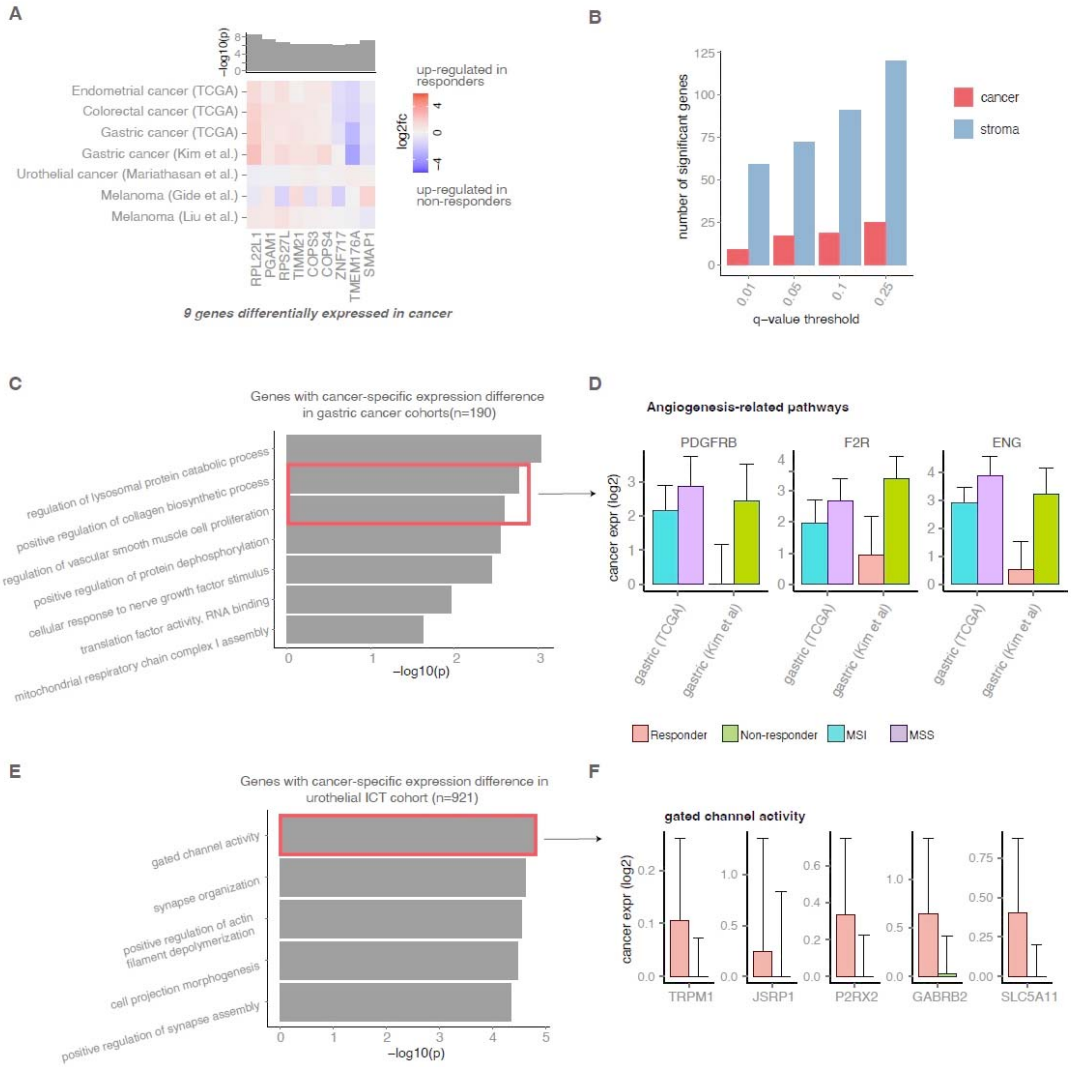

Figure 4. **Differentially expressed genes between responders and non-responders in the cancer compartment. (A)** Heatmap of genes consistently differentially expressed across discovery cohorts in the cancer cells. Heatmaps are colored by the log2 fold change of gene expression. *P*-values of individual cohorts are combined using the Fisher's method, and the -log10(meta p-value) is presented in the bar plot. Genes with q-value<0.01 and *p*-value<0.1 at least 1 ICB cohort are shown. **(B)** Bar plot shows the number of significant genes found in the stroma and cancer compartment at different q-value cutoffs. Pathway analysis of genes with cancer-specific expression differences in **(C)** gastric cancer and **(E)** urothelial cancer. Bar plots of deconvoluted cancer expression of differentially expressed genes in the top enriched pathway in **(C)** gastric cancer and **(E)** urothelial cancer. Error bars represent estimated standard error.

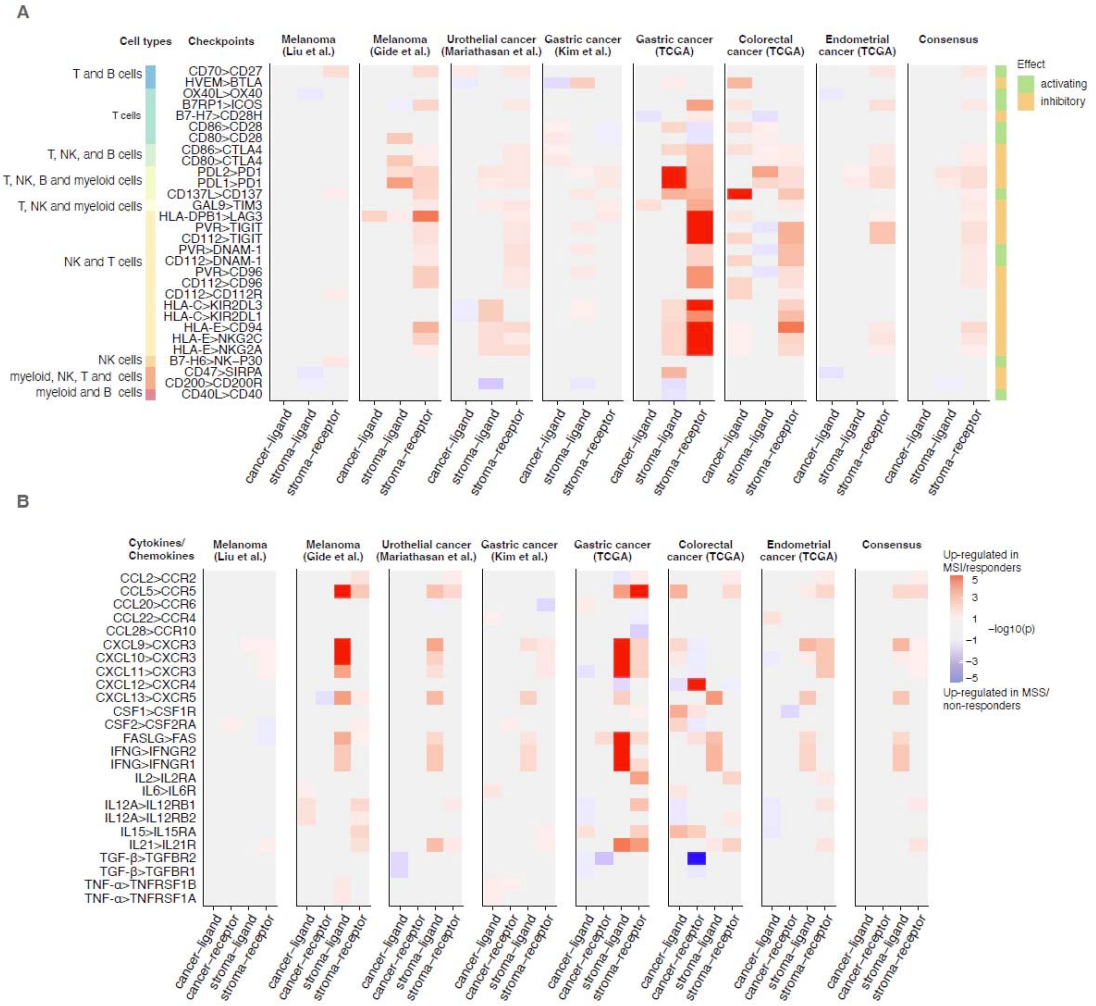

Figure 5. **Analysis of ligand and receptor expression of immune modulators.** Heatmaps of the inferred ligand and receptor expression in the cancer and stroma compartments for **(A)** immune checkpoint proteins and **(B)** cytokines. Heatmaps are colored by the signed -log10(*p*-value) of differential expression.

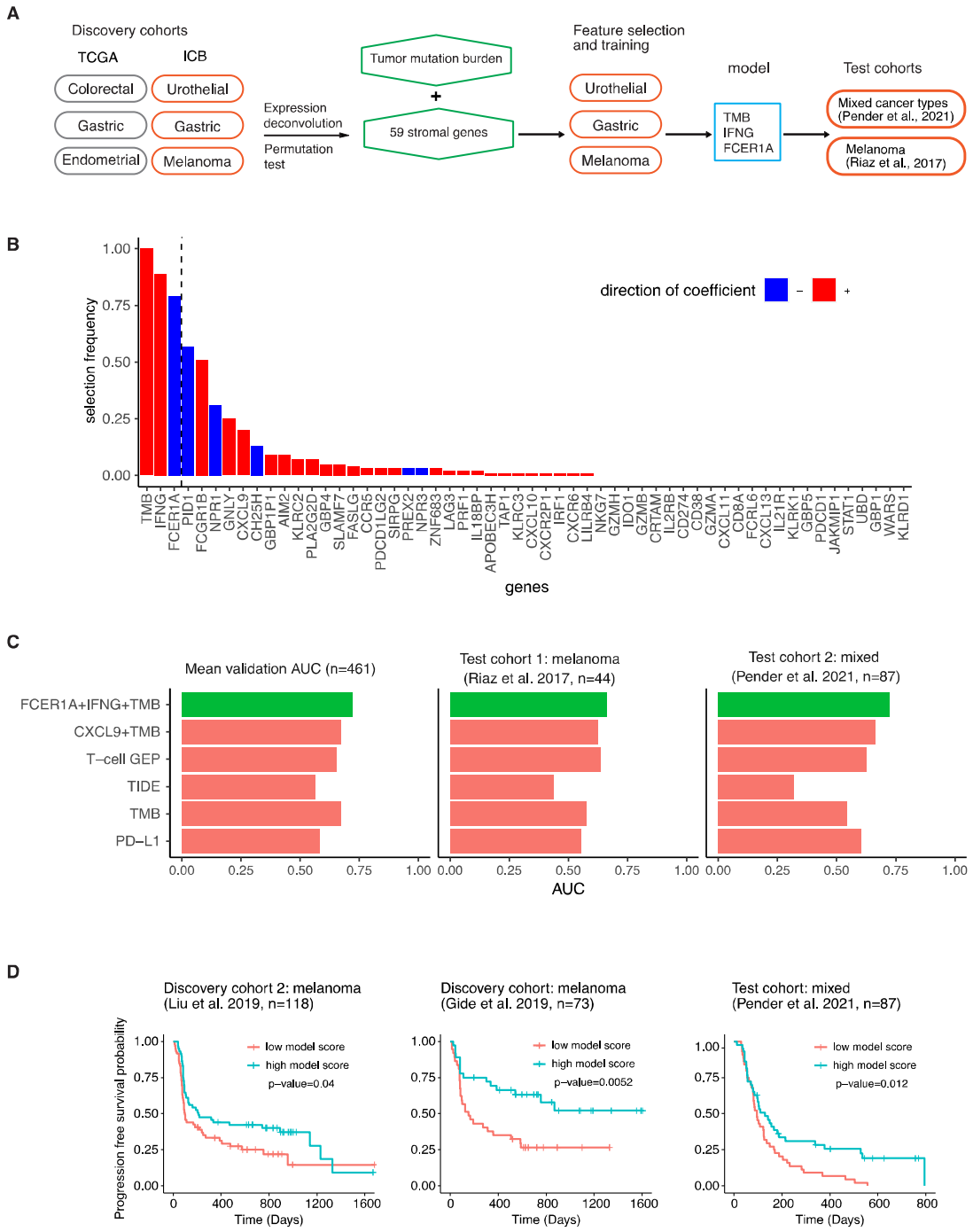

Figure 6. **Predictive modeling of response to immune checkpoint inhibition. (A)** Schematic of data and methods used in model training and testing. **(B)** Top ranked features of ICB response selected by LASSO logistic regression. **(C)** Comparisons of the performance of the TMB+*IFNG*+*FCER1A* model and existing biomarkers in 2 independent test cohorts. **(D)** Kaplan-Meier curves of progression free survival for patients with high vs low predicted scores (greater than or less than median); p-values from log-rank test shown.

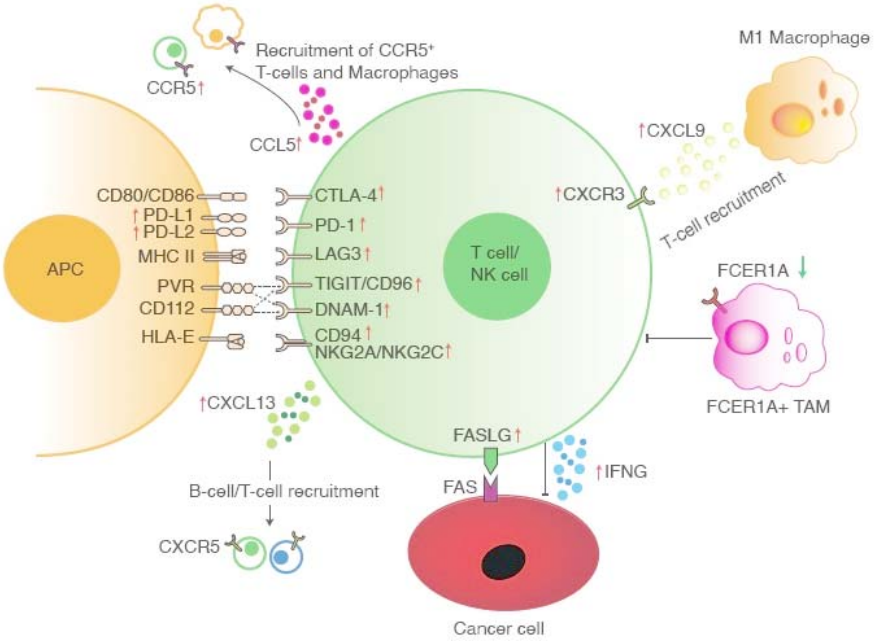

Figure 7. Schematic summarizing the key components associated with ICB response. Red arrows indicate gene positively correlated with ICB response. Green arrow indicates gene negatively correlated with ICB response.